Cholera Toxin Binding Affinity and Specificity for Gangliosides Determined by Surface Plasmon Resonance†

Geoffrey M. Kuziemko, Mark Stroh, and Raymond C. Stevens*

Department of Chemistry, University of California—Berkeley, and Materials Science Division, Lawrence Berkeley National Laboratory, Berkeley, California 94720

Received September 27, 1995; Revised Manuscript Received January 22, 1996⊗

ABSTRACT: The present study determines the affinity of cholera toxin for the ganglioside series GM1, GM2, GM3, GD1A, GD1B, GT1B, asialo GM1, globotriosyl ceramide, and lactosyl ceramide using real time biospecific interaction analysis (surface plasmon resonance, SPR). SPR shows that cholera toxin preferably binds to gangliosides in the following sequence: GM1 > GM2 > GD1A > GM3 > GT1B > GD1B > asialo-GM1. The measured binding affinity of cholera toxin for the ganglioside sequence ranges from 4.61×10^{-12} M for GM1 to 1.88×10^{-10} M for asialo GM1. The picomolar values obtained by surface plasmon resonance are similar to K_d values determined with whole-cell binding assays. Both whole-cell assays and SPR measurements on synthetic membranes are higher than free solution measurements by several orders of magnitude. This difference may be caused by the effects of avidity and charged lipid head-groups, which may play a major role in the binding between cholera toxin, the receptor, and the membrane surface. The primary difference between free solution binding studies and surface plasmon resonance studies is that the latter technique is performed on surfaces resembling the cell membrane. Surface plasmon resonance has the further advantage of measuring apparent kinetic association and dissociation rates in real time, providing direct information about binding events at the membrane surface.

The binding of bacterial toxins to ganglioside receptor GM1[1] is a paradigm for protein−sugar interactions. GM1 is a receptor for the organism *Salmonella typhimurium* (Finklestein et al., 1983), the enterotoxin from *Camplyobacter jejuni* (Walker et al., 1981), and the *Escherichia coli* heat-labile enterotoxin (Donta & Vinter, 1975). However the best-characterized interaction is the one between GM1 and the enterotoxin from *Vibrio cholerae*, cholera toxin (Cuatrecasas, 1973a,b; Holmgren et al., 1973; Staerk et al., 1974; Fishman et al., 1978). Cholera toxin (CT) consists of one A subunit (M_r 27 kDa), responsible for catalysis, and five B subunits (M_r 11.6 kDa), which define the binding region. Intoxication is initiated when the B subunits recognize and bind to the pentasaccharide moiety of GM1 (Eidels et al., 1983). By an unresolved mechanism, the A subunit enters the cell and ADP-ribosylates the signal transduction protein G_s-α. Since ADP-ribosylation of G_s-α abolishes GTP hydrolysis, G_s-α remains constitutively active, resulting in greater intracellular levels of cAMP (Cassel & Pfeuffer, 1978). Elevated cAMP concentrations in the small intestine lead to fluid loss and, if unremedied, death.

The interaction between CT and GM1 has been explored using a variety of techniques: ^{125}I-labeled CT binding to whole fat cells and isolated membranes (Cuatrecasas, 1973a,b); ^{125}I-labeled CT binding to intestinal cells (Holmgren et al., 1975); radiolabeled immunoassays (Fukuta et al., 1988); and isothermal titration calorimetry of CT binding to GM1 incorporated into lipid vesicles (Masserini et al., 1992). The dissociation constants obtained from these studies range from 4.6×10^{-10} M (Cuatrecasas, 1973a) to 5×10^{-8} M (Masserini et al., 1992). Although the contribution of individual saccharide residues toward CT binding has been examined using synthetic analogs (Schengrund & Ringler, 1989; Pacuszka et al., 1991; Lanne et al., 1994), the results are ambiguous and merely point to the importance of the terminal galactose and sialic acid residues.

The importance of these terminal residues is illustrated by the crystal structure of the CT binding domain complexed with GM1 (Merritt et al., 1994). The binding site specificity of CT for GM1 is allocated to the sialic acid (43% of interactions), the terminal galactose (39% of interactions), and the *N*-acetylgalactosamine (17% of interactions). The majority of CT−GM1 interactions are hydrogen bonds mediated by the sugar hydroxyl groups. On the basis of the crystallographic analysis, the specificity and affinity of CT for GM1 are driven by the hydrogen bonding of the two terminal sugar groups, galactose and sialic acid, in a manner resembling a two-fingered pinch (Figure 1).

Although the affinity of CT for GM1 has been examined, a rigorous investigation of the affinity between CT and other gangliosides has yet to be undertaken. We have determined

† This work was supported by the Director, Office of Energy Research, Office of Basic Energy Sciences, Division of Material Sciences, and the Division of Energy Biosciences of the U.S. Department of Energy Contract No. DE-AC03-76SF0098. Support was also received from the Beckman Foundation Young Investigator Award (R.C.S.) and the NSF Young Investigator Award (R.C.S.).

* Address correspondence to this author at the Department of Chemistry, University of California—Berkeley, Berkeley, California 94720.

⊗ Abstract published in *Advance ACS Abstracts,* May 1, 1996.

[1] Abbreviations: BSA, bovine serum albumin; CT, cholera toxin; globotriosyl ceramide, Gal(α,1-4)Gal(β,1-4)Glc-Cer; asialo GM1, GgOse$_4$Cer; GM1, II^{3}NeuAcGgOse$_4$Cer; GM2, II^{3}NeuAcGgOse$_3$Cer; GM3, NeuAc2-3Galβ1-4Glcβ1-Cer; GD1A, IV^{3}NeuAcII^{3}NeuAcGgOse$_4$-Cer; GD1B, II^3(NeuAc)$_2$GgOse$_4$Cer; GT1B, IV^{3}NeuAcII(NeuAc)$_2$GgOse$_4$-Cer; lactosyl ceramide, Gal(β,1-4)Glc-Cer; ODM, octadecylmercaptan; PT, pertussis toxin; POPC, 1-palmitoyl-2-oleoyl-*sn*-glycero-3-phosphocholine; RU, response unit; SPR, surface plasmon resonance.

S0006-2960(95)02314-2 CCC: $12.00

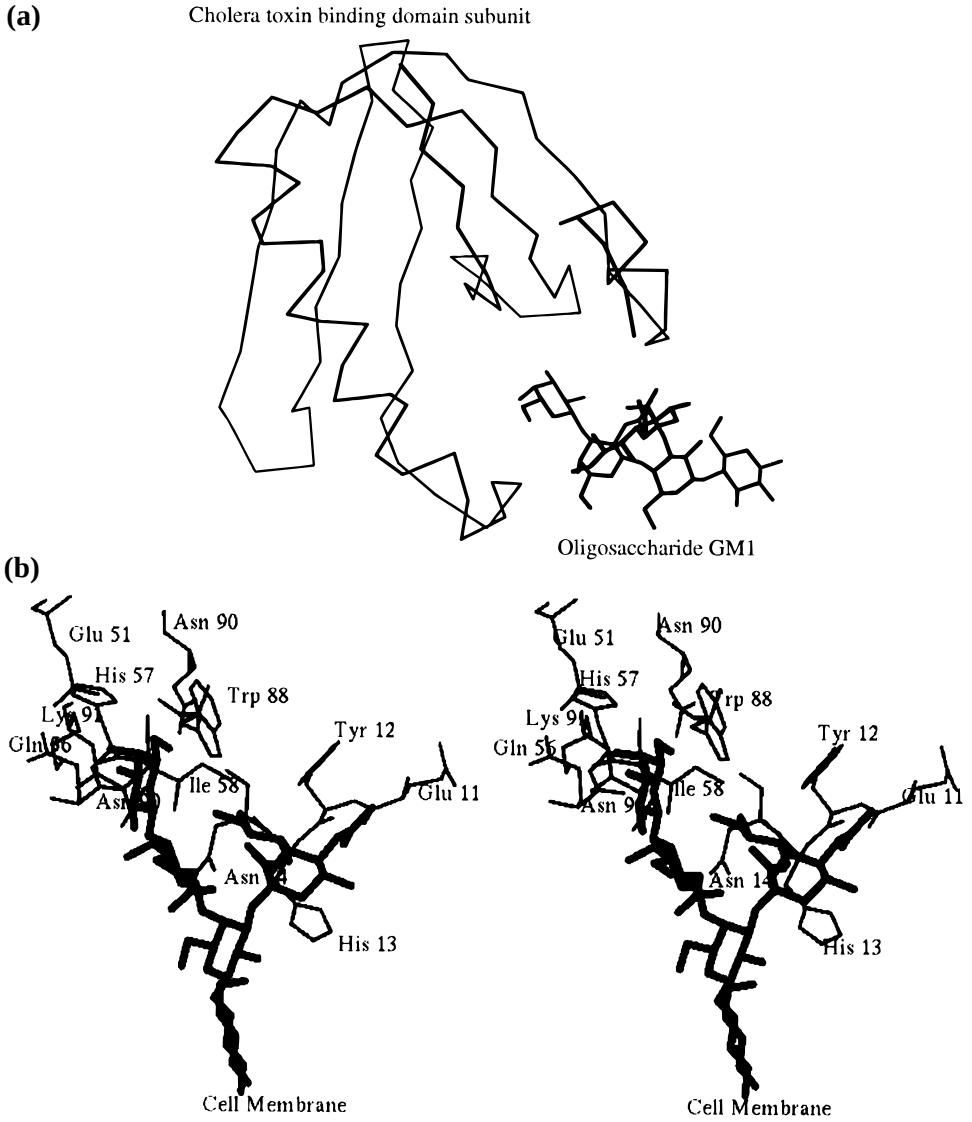

FIGURE 1: (a) Structure of a single CT B subunit binding to the GM1 pentasaccharide (Merritt et al., 1994). (b) Stereoview of the GM1 pentasaccharide inside the CT binding pocket.

CT−ganglioside affinity using a commercial surface plasmon resonance (SPR) device and techniques of self-assembly chemistry. Gangliosides can be self-assembled directly onto the alkylthiol surfaces of a sensor chip, producing an artificial surface similar to a cell membrane. At this artificial membrane, binding interactions are monitored in real time with SPR (Karlsson et al., 1994), which allows direct determination of the apparent kinetic constants, k_a and k_d, for a family of gangliosides.

EXPERIMENTAL PROCEDURES

Equipment and Reagents. Cholera toxin (CalBiochem, La Jolla, CA), pertussis toxin, and bovine serum albumin were purchased and used without further purification (Sigma Chemical Co., St. Louis, MO). Their purity was tested by SDS−PAGE, and their homogeneity was determined by dynamic light scattering (Degiorgio et al., 1980). The lipid 1-palmitoyl-2-oleoyl-*sn*-glycero-3-phosphocholine (POPC) was purchased from Avanti Polar Lipids, Alabaster, AL. All gangliosides GM1, GM2, GM3, GD1A, GD1B, GT1B, asialo GM1, globotriosyl ceramide, and lactosyl ceramide (Figure 2) were purchased from Matreya, Inc. (Pleasant Gap, PA) and used without further purification. The GM1 pentasaccharide salt was purchased from Alexis Biochemicals (San Diego, CA).

The SPR device used for the binding studies was a BIAcore 2000 (Pharmacia Biosensor, Piscataway, NJ). The experimental setup is shown in Figure 3. Two different sensor chips were used in the analysis (stripped/modified CM5 grade sensor chip and a prototype K sensor chip). Each chip contained four flow cells of dimensions ($l \times w \times h$) $2.4 \times 0.5 \times 0.05$ mm. The probing spot for the SPR signal was an active area approximately 0.15 mm^2 in the center of the flowcell (Sjölander & Urbaniczky, 1991).

Homogeneity of Toxin Sample. The diffusion coefficient of CT was measured, and its globular radius was determined using dynamic light scattering (Degiorgio et al., 1980) on a Dyna-Pro 801 Molecular Size Detector (Biotage Inc., Charlottesville, VA). Since the binding domain of CT is larger that the catalytic domain, the globular radius for the entire CT should be similar to the globular radius of the binding domain. Based on the crystal structure (Merritt et al., 1994), the radius of the five-subunit binding domain is 30 Å × 15 Å and should therefore yield an overall globular radius of approximately 30 Å (the radius of the largest dimension). Using the Dyna-Pro, the globular radius was calculated to be

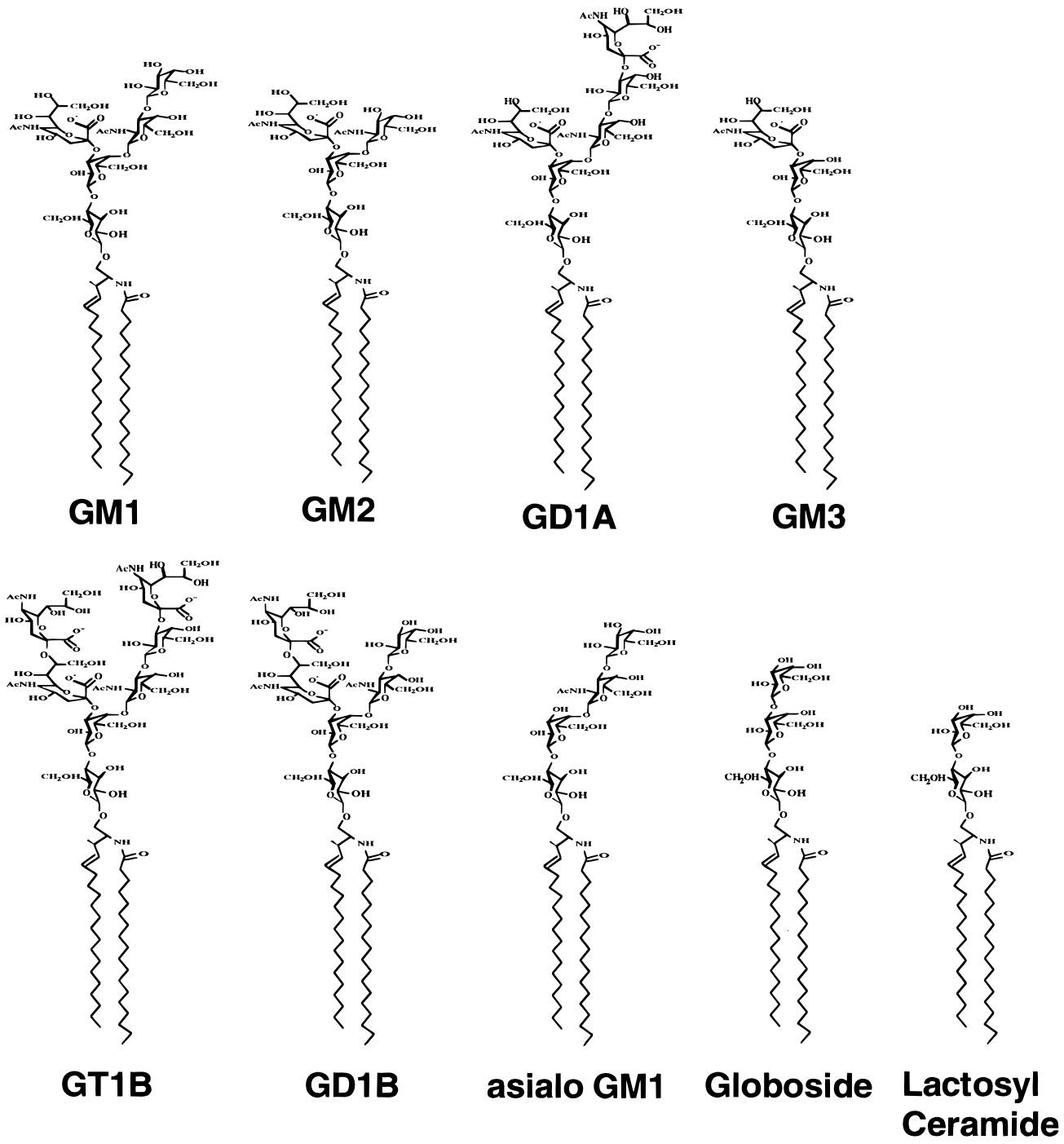

FIGURE 2: Structural relationship of the gangliosides under investigation.

37 Å. Agreement between crystallographic and light scattering data indicates that the CT sample is homogeneous and monodisperse.

Surface Plasmon Resonance. The application of SPR to monitor association and dissociation events is gaining widespread use in the field of biological recognition (Karlsson et al., 1994). Comparisons between SPR and radioligand binding assays show nearly identical values (Payne et al., 1993). SPR occurs when incident light couples to the free oscillating electrons (plasmons) in a thin gold film coated onto a glass support of the sensor chip. Since the resonance angle of the incident light is a function of the refractive index at the gold surface, and the refractive index is sensitive to changes in mass, any binding alters the resonance angle (Kooyman, 1988). A change in surface protein concentration of $\sim$1 ng/mm^2 is followed by a resonance angle shift of 0.1° and a change in 1000 resonance units (RU's) (Stenberg et al., 1990).

BIAcore Kinetic Theory. The BIAcore kinetic theory outlined below holds when the mass transport kinetics of an analyte to a surface bound ligand is faster than the interaction-controlled kinetics between analyte and ligand. The simple, homogeneous interaction considered first is

$$A + B \Leftrightarrow AB \quad (1)$$

where A is defined to be the analyte and B is the ligand immobilized to the sensor chip. We model the rate of

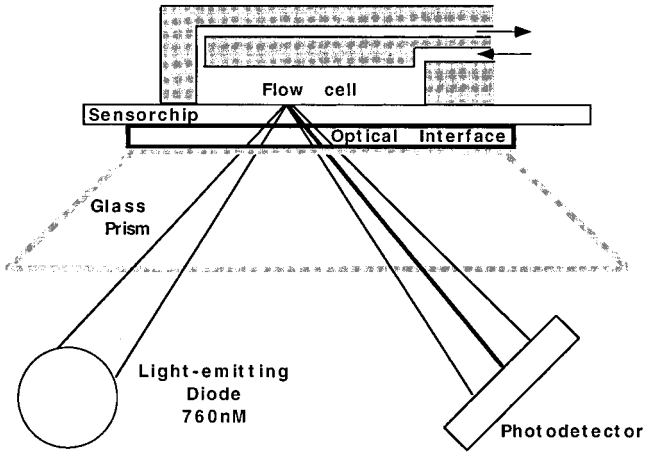

FIGURE 3: Diagram depicting the experimental setup for SPR. The dimensions of the flow cell and the SPR probing area are mentioned in the text.

association and dissociation with eq 2

$$d[AB]/dt = k_a[A][B] - k_d[AB] \quad (2)$$

defining k_a and k_d as the association and dissociation rate constants, respectively. Equation 2 can be expressed in terms of the SPR signal as

$$dR/dt = k_a C R_{max} - (k_a C + k_d)R \quad (3)$$

where R is the SPR signal in RU at time t, dR/dt is the SPR signal's rate of change, R_{max} is the maximum analyte binding capacity in RU, and C is the concentration of injected analyte. Since the sample of analyte is continuously injected over the sensor surface, the concentration of sample in contact with the surface is assumed to be constant. Equation 3 is integrated to give eq 4, which may be used directly for nonlinear regression analysis.

$$R = (1 - \exp\{-(k_a C + k_d)t\})k_a C R_{max}/(k_a C + k_d) \quad (4)$$

After injection of analyte, the concentration (C) is set to zero in eq 3, and the dissociation phase is modeled with eq 5.

$$dR/dt = -k_d R \quad (5)$$

The integrated form of eq 5 can also be used directly for nonlinear regression analysis.

$$R = R_o \exp\{-k_d(t - t_o)\} \quad (6)$$

While the theory presented above illustrates the behavior of an ideal system, several factors complicate the kinetic analysis of CT−ganglioside interactions: (1) The binding domain of CT is pentameric; thus, the five binding sites may behave in a cooperative fashion and enhance the rate of association by an avidity effect. (2) The pentameric binding domain may sterically hinder interactions with multiple gangliosides. (3) When association rates are very rapid, $k_a = 10^5$ or greater, diffusion can limit the association kinetics. (4) Rapid association rates favor the re-association of analyte to the chip during the dissociation phase (rebinding). (5) Finally, homogeneity of the ligand and analyte is critical in determining both the association and dissociation constants.

Preparation of Sensor Chips. Initial studies of the CT−GM1 interaction were carried out with stripped and modified hybrid phospholipid-containing bilayer membranes incorporated with the ganglioside GM1 (Plant et al., 1995). A CM5 sensor chip was soaked in ethanol to dissolve the adhesive, and the gold chip was removed from the Pharmacia Biosensor Chip Assembly. The gold surface was stripped and reconditioned by placing it in a PDC-236 plasma cleaner (Harrick Corp., Ossining, NY) for 5 min, and the chip was subsequently soaked in a 10 mL solution of 0.1% octadecylmercaptan (ODM) in ethanol for 18 h. A lipid solution was made by dissolving 5 mole % GM1:95 mole % POPC in 2 mL of chloroform:methanol (2:1), evaporating the solvent using a stream of argon gas, and shaking vigorously with 2 mL of ddH_2O. (While a range of GM1−POPC solutions was tried, 5 mole % GM1 was the lowest concentration of ganglioside that gave analyzable kinetic data.) The gold chip treated with ODM solution was rinsed with ethanol followed by ddH_2O and submerged overnight in the lipid solution. After rinsing with ddH_2O and reattaching to the holder using silicon adhesive, the gold chip was ready to use.

Subsequent experiments, including all of the kinetic measurements, were performed with Pharmacia Biosensor prototype K chips (kindly provided by Pharmacia Biosensor, Piscataway, NJ). Type K chips lack the carboxy-methylated dextran mesh found on CM5 chips and consist of a ODM layer preattached to the gold surface. We conditioned the type K chips by preparing the 5 mole % GM1:95 mole % POPC solution as mentioned above, adding 50 μL of the ganglioside solution and 50 μL of ddH_2O directly to the gold surface and letting the chip self-assemble in a humid environment overnight. The chip surface was rinsed with ddH_2O and was ready for use in the BIAcore 2000.

BIAcore Experiments. Initial monitoring of CT and control molecules was performed on a single flowcell with a BIAcore programmable method. This method used CT concentrations ranging from 60 to 2400 nM in 10 mM Trizma, pH 7.5, 150 mM NaCl, 2 mM EDTA at a constant flow rate of 40 μL/min for 13 min, with 40 μL of toxin injected at the start of each run. The sensor chip surface was regenerated, and bound toxin was removed by injection of 40 μL of 4.4 M $MgCl_2$. All samples were filtered (0.2 μm) and thoroughly degassed. Subsequent measurements for kinetic analysis used all four flow cells to collect data over a concentration range from 120 to 240 nM. To determine the degree of rebinding, a series of flow rate experiments were conducted with 240 nM CT at 5, 10, 20, 40, 60, and 80 μL/min. An additional check for rebinding involved coinjecting CT with an excess of soluble GM1 pentasaccharide (62.5 μM) at 40 μL/min.

Ganglioside Screening. All gangliosides, globotriosyl ceramide, and lactosyl ceramide were self-assembled on type K chips using the methods described above for the self-assembly of the POPC−GM1 monolayer. All ganglioside vesicle solutions were prepared with 5 mole % ganglioside: 95 mole % POPC.

Competition Assay. To examine if the interaction between CT and immobilized ganglioside could be competed away, CT samples were incubated with 100 mM solutions of soluble GM1, sialic acid, and lactose. Before injection 100 μL samples of CT ranging from 60 to 960 nM were incubated

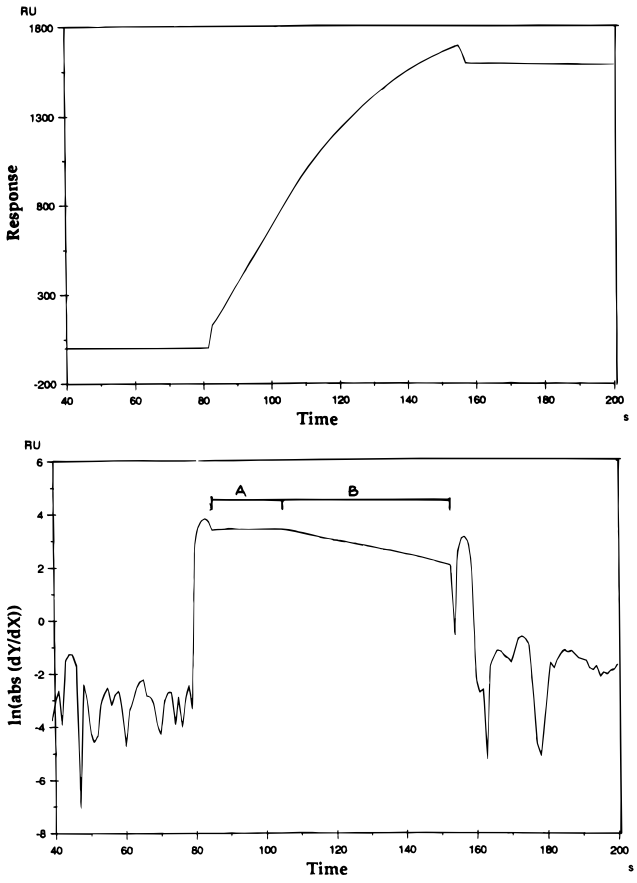

FIGURE 4: (a) Typical sensorgram of CT binding to the GM1 surface. (b) The same sensorgram viewed as a graph of ln[abs(d*R*/d*t*)] versus time. The flat portion designated by A represents mass transport-limited data. The sloping portion under B represents interaction-limited data.

with 100 μL of competitor for 15 min at 25 °C and analyzed on the BIAcore using the standard method described above.

Data Analysis. We began analysis of the sensorgrams by viewing each curve with a data transform provided in the BIAcore Evaluation software, v2.1. This data transform plots each curve as ln[abs(d*R*/d*t*)] versus *t*, where d*R*/d*t* is the change in SPR signal response per change in time (Figure 4). Since this function is linear for homogeneous 1:1 association, it can be used to distinguish regions of mass transport-limited kinetics from reaction-limited kinetics (BIAcore Manual). All data from each curve were selected from the reaction-limited kinetics regime. We analyzed CT binding data through nonlinear curve fitting of individual sensorgrams to minimize errors associated with a linear transform of sensorgrams (O'Shannessy et al., 1993). After the base lines of all sensorgrams in each flow cell were averaged, the apparent dissociation constant was determined by fitting each curve to a biphasic exponential decay function. On the basis of this dissociation constant and the concentration of each sample, an exponential function for the apparent association constant was extracted. All curve fitting was performed, using the Marquardt−Levenberg algorithm (BIAevaluation package, version 2.1, provided by Pharmacia Biosensor).

RESULTS

Binding of CT to GM1 Sensor Chips. Figure 5 is a typical sensorgram generated from the injection of 30−2400 nM

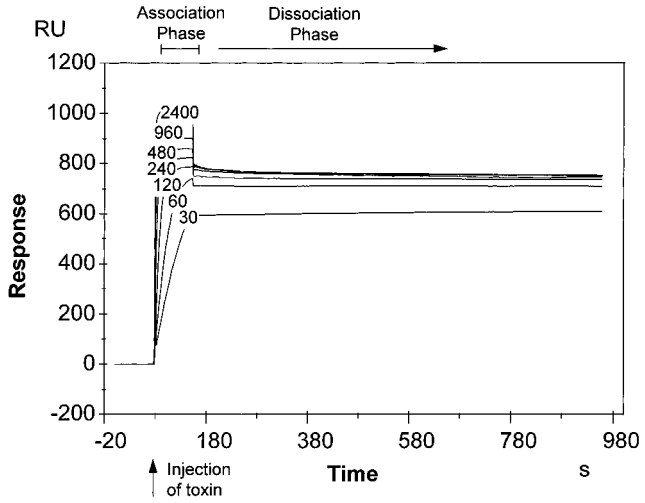

FIGURE 5: Sensorgram (response in RU versus time in s) obtained for 30, 60, 120, 240, 480, 960, and 2400 nM CT injections across a self-assembled 5 mole % GM1:95 mole % POPC sensor chip. Association and dissociation phases are as indicated. R_{max} is noted to be approximately 800 RU.

CT across a 5 mole % GM1 sensor chip. Steep curvature for the association phase and a very shallow slope for the dissociation phase were observed to correspond with fast association and slow dissociation rates respectively. The CT−GM1 response is very large in magnitude, with an R_{max} value of roughly 800 RU.

Stability of Modified Sensor Chips. The sensor chip was exposed to multiple regenerations during the course of an automated method, with each method spanning up to 3 h in duration. Since one sensor chip was used for up to four methods, the integrity of the sensor chip surface is crucial for reliable results. The response is proportional to the total mass of material on the surface of the sensor chip; any net decrease in base line with time indicates the potential loss of ligand. The base line was noted to maintain its value for the duration of each automated method, controlling for ligand loss. If no ligand was lost during a method, then injection of identical concentrations of CT across the sensor chip should give the same binding curve. For this reason, all methods were initiated and concluded with the same concentration of CT.

Specificity of Binding. Specificity of the interaction was addressed in two ways: (1) the degree of nonspecific binding of CT to POPC was determined; (2) the degree of specific binding of control proteins to immobilized GM1 was also determined. Injections of 30−2400 nM CT across a POPC surface increased the base line by 10−50 RU, indicating a small nonspecific response. However, when CT was injected over a POPC−GM1 surface, the increase in base line was approximately 800 RU (Figure 5), demonstrating a large specific binding. Although the system demonstrated specific binding to GM1, this small nonspecific interaction between CT and POPC prompted us to use a biphasic dissociation model in our analysis. When bovine serum albumin (BSA) and pertussis toxin (PT) were injected over a POPC/GM1 surface, the change in base line was approximately zero (Figure 6a,b). Thus proteins lacking GM1 specificity produce a negligible binding response.

Determination of Kinetic Constants. We determined that the simple monophasic model outlined above was the best

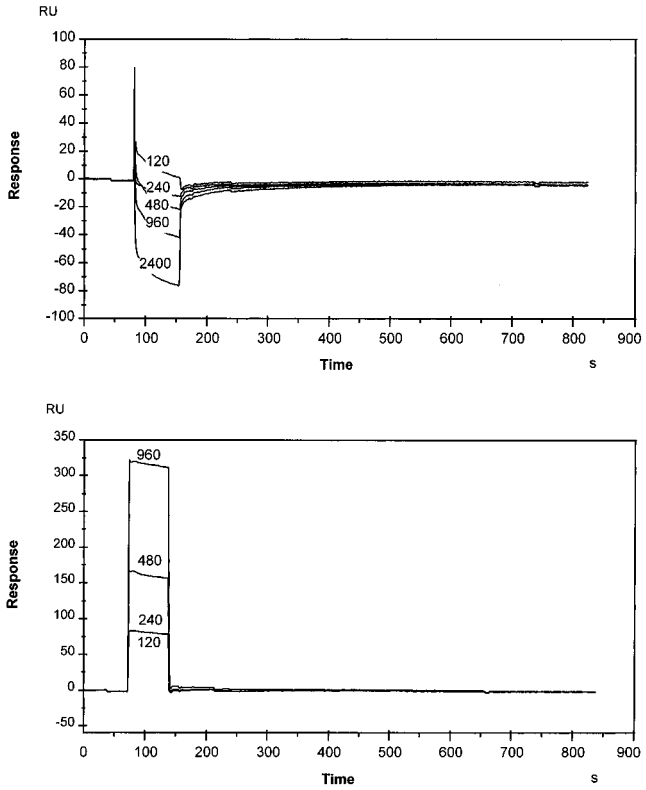

FIGURE 6: Sensorgrams (response in RU versus time in s) of 5 mole % GM1:95 mole % POPC self-assembled sensor chips for (a) 120, 240, 480, 960, and 2400 nM bovine serum albumin and (b) injections of 120, 240, 480, and 960 nM pertussis toxin. Sensorgrams a and b demonstrate bulk refractive changes only (in a, we have a negative bulk refractive index change) with subsequent R_{max} values close to zero; no substantial binding occurs.

description of the association data based on the criterion of residual plots. Residual plots depict the differences between the data and the calculated fit. The data will poorly fit the model if the residuals vary systematically, or if their magnitude exceeds machine noise. Upon comparing the residuals for the biphasic against the monophasic association models, we observed no difference in the magnitude or variation. Another indication that monophasic association was appropriate comes from examining a plot of k_s vesus C. The quantity k_s is defined to be $k_aC + k_d$ and was determined with version 2.1 of the BIAevaluation software. Since the first derivative of k_s with respect to C is k_a, the second derivative is zero for a monophasic system; concavity in a plot of k_s versus C reveals the inappropriateness of a monophasic fit. Using the BIAsimulation software provided by Pharmacia BIAcore, three hypothetical k_s versus C plots were constructed (Figure 7a): the top curve is for a system with heterogeneous ligands (1:9 ratio of ligands with K_d's of 10^{-6} and 10^{-12} M, respectively); the middle curve represents the monophasic system in eq 1 with k_d and k_a of 1×10^6 s^{-1} and 1×10^{-6} M^{-1} s^{-1}, respectively (ideal case); the bottom curve represents a similar system, except the analyte occupies three ligand sites (steric hindrance). Note that the middle curve is linear in C, while the two other plots are curved. A plot of k_s vs C for the CT−GM1 system is characterized by random scatter about a straight line (Figure 7b). Thus the association phase appears to be monophasic.

For the dissociation phase of the CT−GM1 sensorgrams, it is apparent that a monophasic model is inappropriate. From eq 6, we note that a plot of $\ln(R/R_o)$ vs $(t - t_o)$ should give

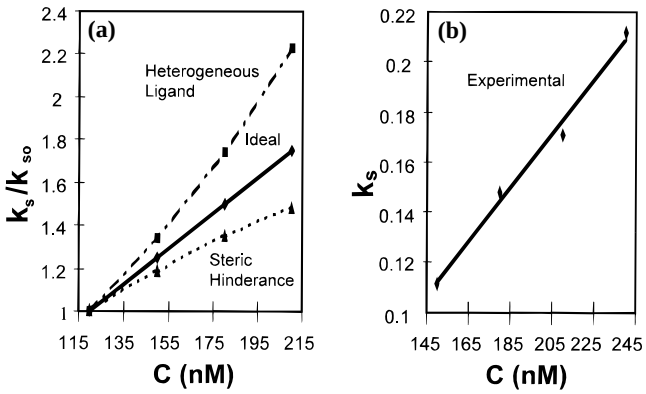

FIGURE 7: (a) Plots of k_s/k_{so} (division by k_{so}, the value of k_s at C = 120 nM, scales all curves to an initial value of 1) versus concentration (nM) generated via BIASimulation for three hypothetical situations: the upper dashed/solid curve represents the case where one analyte molecule occupies three ligand sites, the lower dashed curve illustrates the effect of heterogeneous ligand (1:9 ratio of ligands with K_d values of 10^{-6} and 10^{-12} M, respectively), and the middle, solid straight line represents the ideal case with neither steric hindrance nor ligand heterogeneity. For both the upper multiple-site and the middle ideal situation, k_a and k_d equal the maximum experimental values of 1×10^6 M^{-1} s^{-1} and 1×10^{-6} s^{-1}, respectively. (b) Plot of k_s versus concentration for actual data obtained from a typical trial with a 5 mole % GM1:95 mole % POPC self-assembled sensor chip where we find random scatter about a straight line.

a straight line with slope $-k_d$ for a monophasic interaction. Such a plot is provided in Figure 8a, where the curves are seen to be nonlinear. In the biphasic model, the total signal R is split into two components, R_1 and R_2, representing separate interactions with dissociation constants of k_{d_1} and k_{d_2}, respectively. Support for a biphasic model comes from an examination of the residuals associated with the monophasic versus the biphasic fit (Figure 8b,c). We selected the biphasic model as the appropriate model since residuals are both maximized in randomness and minimized in magnitude.

A monophasic association phase and a biphasic dissociation phase can be explained as follows. For a system with two ligands, the SPR signal in the association phase is resolved into two components, R_1 and R_2, as was done for the dissociation phase. The sum of R_1 and R_2 gives the total response R. The SPR response is given in eq 4. We rearrange eq 4 by dividing both numerator and denominator by k_aC and arrive at an expression for either R_1 or R_2:

$$R_i = (1 - \exp\{-(k_{a_i}C + k_{d_i})t\})R_{max,i}/(1 + k_{d_i}/k_{a_i}C) \quad (7)$$

where $i = 1$ or 2 and k_{a_i}, k_{d_i}, and $R_{max,i}$ correspond to the association and dissociation constants and maximum response for ligand i.

For chips with only a POPC surface, the maximum response falls between 10 and 50 RU. In the limit where k_{a_i} tends to infinity in eq 7, then $R_i = R_{max,i}$. For a system in which R_1 corresponds to the nonspecific interaction between CT and POPC and R_2 corresponds to the GM1−CT interaction, the total response R is approximated by eq 8.

$$R = R_{max,1} + (1 - \exp\{-(k_{a_2}C + k_{d_2})t\})R_{max,2}/(1 + k_{d_2}/k_{a_2}C) \quad (8)$$

Since $R \gg R_{max,1}$ (R = 800 RU, R_i = 10−50 RU) for the majority of the association phase eq 9 gives a final ap-

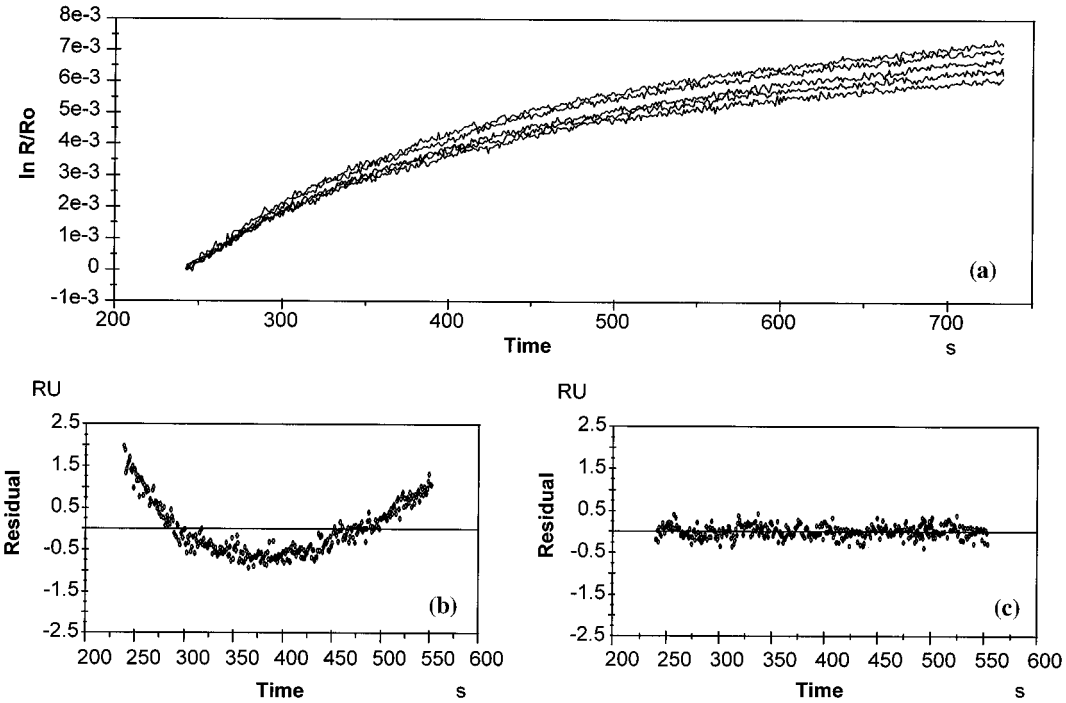

FIGURE 8: (a) Plot of ln (where R_o is the response at $t = 250$ s) versus time for the dissociation phase of 120, 150, 180, 210, and 240 nM CT over a 5 mole % GM1:95 mole % POPC self-assembled sensor chip. Residuals versus time for (b) monophasic fitting and (c) biphasic fitting. The curved nature of the plot leads to systematic deviations in the calculated versus actual data. Biphasic fitting gives residuals that are reduced in magnitude and deviations that are not systematic.

Table 1: Kinetic and Thermodynamic Binding Constants for Cholera Toxin Injected over Various Immobilized Gangliosides (5 mole % Ganglioside:95 mole % POPC, Micellar Concentration)

ganglioside	n^a	k_a ($\times 10^{-6}$ M^{-1} s^{-1})	k_{d_1} ($\times 10^{3}$ s^{-1})	k_{d_2} ($\times 10^{5}$ s^{-1})	$K_d{}^b$ ($\times 10^{12}$ M)	95% CI[c]
GM1	48	1.27	8.92	0.586	4.61	0.63
GM2	12	2.94	6.21	4.34	14.7	2.8
GD1A	16	1.88	6.38	5.98	31.8	4.2
GM3	12	1.93	5.25	15.3	79.3	7.8
GT1B	12	0.815	6.09	13.6	167	19
GD1B	16	0.789	4.98	14.1	179	19
Asialo-GM1	12	0.970	6.15	18.3	188	47
globotriosyl ceramide[d]	16					
lactosyl ceramide[d]	16					
POPC only[d]	32					

[a] n refers to the total number of observations. [b] K_d is calculated from the ratio of k_{d_2} to k_a, since we attribute k_{d_1} to a nonspecific interaction. [c] 95% CI refers to the 95% confidence interval for the given number of observations. [d] Globotriosyl ceramide, lactosyl ceramide, and POPC display immeasurably fast on-rates, irregular off-rates, and R_{max} values of 10−50 RU, indicative of nonspecific interactions.

proximate expression for R.

$$R - R_{max,1} \cong R = (1 - \exp\{-(k_{a_2}C + k_{d_2})t\})R_{max,2}/(1 + k_{d_2}/k_{a_2}C) \quad (9)$$

Equation 9 describes a monophasic association and has been used to calculate the constants listed in Table 1.

To further support the notion that R_1 is due to a nonspecific interaction, we turn to the data obtained for non-GM1 gangliosides. Table 1 reveals that k_{d_2} varies from 0.586×10^{-5} to 18.3×10^{-5} s^{-1} (a 31-fold range) over all the gangliosides. If k_{d_1} represented a specific interaction, then it should vary with the different gangliosides. However, variation in k_{d1} is only from 4.98×10^{-3} to 8.92×10^{-3} s^{-1} (a 2-fold range) and is the same order of magnitude as the k_d for the CT−POPC interaction. Furthermore, for every ganglioside, the value of R_1 accounts for less than 10% of the total response, R. Consequently k_{d_1} is used to describe nonspecific interactions, while k_{d_2} is used as the CT−ganglioside dissociation constant.

Two additional factors (mass transport and rebinding) relevant to the analysis were addressed in the following manner. As mentioned before, all sensorgrams were viewed with a derivative transform (Figure 4) that allows one to discern mass transport and kinetic regimes. Only sensorgrams with data in the kinetic regime were used for analysis. We also examined the k_d for CT/GM1 binding over a range of flow rates (5, 10, 20, 40, 60, and 80 μL/min). Our analysis showed no dependence of k_d upon flow rate, indicating little influence of mass transport on CT−GM1 binding. We chose high buffer flow rates and low ligand surface concentrations to lower mass transport and rebinding. Accordingly the CT experiments were performed with a buffer flow rate of 40 μL/min and a 5 mole % GM1 micellar concentration for self-assembly of the surface.

We also analyzed the early portion of each dissociation phase to obtain dissociation constants at which the rebinding would be smallest. As the dissociation phase progresses, more ligand sites become available for rebinding; therefore, data from the early portion of the dissociation would be less

Table 2: Resultant Kinetic and Thermodynamic Constants after Incubation with 100 mM Soluble Competitor

soluble competitor	n	k_a ($\times 10^{-6}$ M^{-1} s^{-1})	k_{d_1} ($\times 10^{3}$ s^{-1})	k_{d_2} ($\times 10^{5}$ s^{-1})	K_d ($\times 10^{12}$ M)	95% CI
GM1	16	0.567	8.79	43.3	764	440
lactose	16	0.378	8.31	1.10	29.1	8.8
sialic acid	16	0.404	8.26	1.41	34.9	9.1

influenced by rebinding. Rebinding effects appear in the analysis as changes in the k_d that directly vary with C and as residuals of increasing size. In our analysis the dissociation constants were not noted to be increasing functions of C, while residuals remained random and within instrument noise.

As a final check for the effects of rebinding, we compared the sensorgrams of CT−GM1 with CT−GM1 co-injected with an excess of the soluble GM1 pentasaccharide (62.5 μM). If rebinding dominated the CT−GM1 interaction, then sensorgrams injected with the soluble GM1 pentasaccharide would exhibit different kinetic constants: the soluble GM1 pentasaccharide would bind to dissociating CT, prevent rebinding, and ultimately exhibit an altered k_d. Comparison of the CT−GM1 sensorgrams with the CT−GM1−soluble GM1 pentasaccharide sensorgrams revealed similar kinetic constants. Thus rebinding appeared to play a minimal role in our experiments.

Determination of K_d. The BIAcore 2000 has the capacity to run and monitor four flow cells simultaneously in a given automated method. Therefore, four sets of data were collected for each concentration of CT. A typical method would incorporate five separate bulk concentrations of CT. We know from the Arrhenius correlation that kinetic constants may not be functions of either ligand or analyte concentrations. Assuming similar conditions between flow cells, all kinetic constants were averaged regardless of flow cell and bulk concentration, thereby obtaining a sample standard deviation. K_d was determined as the ratio of apparent k_{d_2} to k_a.

With the same general method established for the analysis of the CT−GM1 system, apparent kinetic and thermodynamic constants were determined for a series of gangliosides, and the effects of soluble competitors were determined. All systems except for CT−GM1 contained approximately 16 observations (the CT−GM1 system had 48 observations). The fewer the observations, the less reliable the mean. In order to rank the corresponding average values for K_d among the alternate gangliosides, it is important to know the location of the true mean (the mean value at infinite observations). While the sample standard deviation gives the breadth of the distribution, the confidence interval relates probability of finding the true mean within a given range. For this reason the 95% confidence interval, as opposed to the standard deviation, is given as the uncertainty measure in all calculated values of K_d.

CT Binding to Ganglioside Series. Although the apparent kinetic and thermodynamic constants for the interactions between CT and the gangliosides are similarly high, certain differences can be detected (Table 1). The apparent association constants for GM1, GM2, GD1A, and GM3 are similar, near 2×10^6 M^{-1} s^{-1}. The apparent dissociation constants, however, range from 5.86×10^{-6} s^{-1} (GM1) to 15.3×10^{-5} s^{-1} (GM3). Thus, while CT binds to GM1, GM2, GD1A, and GM3 at approximately the same rate, it is released at different rates. The interactions with GT1B, GD1B, and asialo-GM1 show weaker responses, combining a slower association rate with a faster dissociation rate. Finally, nonspecific responses were found with globotriosyl ceramide and lactosyl ceramide, whose R_{max} values are comparable to those from POPC-only chips (10 RU $\leq R_{max} <$ 50 RU).

Competition Analysis. The incubation of CT with an excess solution of soluble GM1 (100 mM) showed a great decrease in binding to immobilized GM1, altering the K_d from 4.61 ± 0.63 pM to 764 ± 440 pM (Table 2). Incubations with 100 mM lactose and sialic acid solutions produced smaller decreases, raising the K_d from 4.61 ± 0.63 pM to 29.1 ± 8.8 pM and 34.9 ± 9.1 pM, respectively (Table 2).

DISCUSSION

Comparison of Affinities. BIAcore analysis reveals a K_d of 4.61×10^{-12} M for the CT−GM1 system. This affinity is tighter than the value of 4.6×10^{-10} M, found using whole-cell assays (Cuatrecasas, 1973a), and the value of 5×10^{-8} M, calculated by calorimetry (Masserini et al., 1992). The disparity between our SPR results and results found in the literature may exist for several reasons. Although the surface distribution of gangliosides on sensor chips is homogeneous, the population of gangliosides on whole cells is heterogeneous. For example, intestinal mucosal cells contain GM1, GD1, and GT1B (Holmgren et al., 1975). For a mix of gangliosides, binding assays on whole cells would reveal an affinity constant derived from strong binding sites, like GM1, and weaker affinity sites, such as GT1B. This mixed K_d would be larger than the K_d obtained from a homogeneous surface of strong binding sites as found on a sensor chip.

Another possibility for the disparity between calorimetry and SPR data is that immobilization of GM1 onto the BIAcore sensor chip may promote avidity. Avidity is an increase in apparent binding affinity due to the proximity of more than one binding site. While little is known about the avidity of pentavalent CT, a theory has been formulated for bivalent avidity (Crothers & Metzger, 1972; Kaufman & Jain, 1992). If one site of a bivalent molecule binds to an immobilized ligand, and the surface geometry places another ligand within range of the second binding site, then the entropy barrier for the second site to bind an immobilized ligand is greatly reduced. This results in a stronger apparent binding constant (Crothers & Metzger, 1972). Experimental reports on avidity suggest at least a 10-fold difference in affinity between monovalent and bivalent antibodies (Malmqvist, 1994). In the case of polyvalent molecules, such as the pentameric immunoglobulin class M (IgM), the difference is predicted to be 400 times greater (Crothers & Metzger, 1972). Calorimetry uses GM1 incorporated into small unilamellar vesicles (Masserini et al., 1992), which are highly curved. Hence the surface geometry may not promote avidity. Conversely, SPR has GM1 incorporated into a planar surface with low curvature. Thus the SPR surface geometry would be ideal for promoting avidity.

Finally, differences in affinity may arise due to experimental conditions. While SPR analysis of self-assembled surfaces is physically non-invasive, other techniques may subject CT or gangliosides to harsh physical extremes. Binding experiments using radiolabeled CT expose the toxin to potentially denaturing conditions (Cuatrecasas, 1973a). Calorimetry experiments cycle gangliosides, asymmetrically incorporated into lipid vesicles, over a wide range of temperatures (Masserini et al., 1992). Since the values for CT−GM1 as determined by calorimetry are close to those found for CT binding to oligosaccharide−GM1 (Schön & Freire, 1989), calorimetry may produce a population of the oligosaccharide−GM1 from GM1.

Determination of the binding affinities for CT to a series of gangliosides revealed the following sequence of binding strength: GM1 > GM2 > GD1A > GM3 > GT1B > GD1B > asialo GM1 (Table 1). The sequence determined by BIAcore resembles a series based on whole-cell assays (Cuatrecasas, 1973a) and radiolabeled CT assays (Holmgren et al., 1980), which place GM1, GM2, GD1A, and GM3 above GD1B, GT1B, and asialo GM1. However, the BIAcore results differ from a sequence obtained by radiolabeled immunoassays, in which the order was GM1 > GD1B > GM2 > GM3 > GT1B (Fukata et al., 1988).

Correlating Structure and Function. To see if the crystal structure of CT binding domain correlated with BIAcore kinetic results, we performed a CT−GM1 binding experiment with the buffer used to crystallize the binding domain (Merritt et al., 1994). Analysis revealed a K_d of 7.37 ± 3.45 pM, a value within the 95% confidence interval of 4.61 ± 0.63 pM calculated in Table 1. Since the K_d's were similar, we compared the GM1 crystallographic structure (Figure 1b) with BIAcore kinetic data and other functional information extracted from the literature.

We began by examining the terminal galactose residue, which has 39% of interactions in the crystal structure (Merritt et al., 1994). This galactose is pliable to perturbation, even removal, without dramatic effects on affinity. The CT−GM2 interaction is a good example. GM2 is a ganglioside similar to GM1 except that GM2 lacks the terminal galactose. Comparing BIAcore results between GM1 and GM2 only show a 3-fold rise in K_d from 4.61 ± 0.63 pM to 14.7 ± 2.8 pM. Work on fuc-GM1, a GM1 analog possessing an α-fucose linked to the 2-position on the terminal galactose, actually shows a 2-fold stronger K_d (Masserini et al., 1992). Further evidence that perturbing the terminal galactose results only in minor increases of K_d is seen with GD1A. Ganglioside GD1A differs from GM1 by the presence of a second sialic acid linked to the 3-position of the terminal galactose. This addition of another sialic acid only results in a 6-fold weaker K_d, from 4.61 ± 0.63 pM to 31.8 ± 4.2 pM.

Removal of the *N*-acetylgalactosamine (galNAc) adjacent to the terminal galactose results in a larger change in K_d. According to the crystal structure, the galNAc possesses only 17% of all contacts (Merritt et al., 1994). When a sialic acid is added at the C(7) position of galNAc, the binding of CT is barely altered relative to CT−GM1 binding (Schengrund & Ringler, 1989). Yet if galNAc is removed from GM1, as in the case of GM3, BIAcore analysis reveals a 16-fold weaker K_d, from 4.61 ± 0.63 pM to 79.3 ± 7.8 pM.

Changes to the terminal sialic acid of GM1 lead to the largest increases in the kinetic parameters. Elimination of a sialic acid, as with asialo GM1, or addition of a second sialic acid, as with GT1B and GD1B, weakens the K_d from 4.61 ± 0.63 to 167 ± 19, 179 ± 19, and 188 ± 47 pM (decreases of 38-, 34-, and 36-fold respectively). These weaker K_d's are not merely the result of steric hindrance, as the addition of Lucifer Yellow and Rhodamine to the C(7−9) tail of GM1's sialic acid have barely altered CT−GM1 binding (Spiegel, 1985). Deletion of the tail also fails to change binding (Schengrund & Ringler 1989). Therefore an additional sialic acid may disrupt the natural hydrogen bond network by bonding to the carboxylic acid at C(2) in GM1's sialic acid (Lanne et al., 1994).

Correlating the structures of gangliosides (Figure 2) with the kinetic data determined on the BIAcore (Table 1) we can conclude the following: the binding "pinch" between CT and gangliosides is a function of a "thumb" and a two-sugar "finger". Examination of the GM2, GD1A, and GM3 structures reveals that all are modified on the finger composed of the terminal galactose and the adjacent galNAc, leaving the sialic acid thumb unaltered. The association rates for GM2, GD1A, and GM3 are similar to GM1, but the dissociation rates are faster. Meanwhile GD1B, GT1B, and asialo GM1 either lengthen the ganglioside thumb by adding an extra sialic acid or shorten it by removing the existing sialic acid. In both instances, the association rates are lower and dissociation rates are faster when compared to CT−GM1 kinetics. Therefore, while the sialic acid thumb is sufficient for recognition, the terminal galactose and galNAc finger are required to stabilize the CT−ganglioside interaction.

Effect of Competitors. Upon incubating CT with various competitors, we noticed two types of increase in K_d. The first increase occurred with lactose and sialic acid and resulted in a 7-fold weakening in K_d, from 4.61 ± 0.63 to 29.1 ± 8.8 pM and 34.9 ± 9.1 pM, respectively (Table 2). This corresponds to a K_d of 31.8 ± 4.2 pM for GD1A. The k_a for sialic acid and lactose also resembles the k_a of GD1B. Thus competitors may remain lodged in the binding pocket when CT binds. Support for this hypothesis comes from another crystal structure showing the terminal galactose of lactose bound to the B subunit of LT (Sixma et al., 1992). The primary sequence of LT is 80% identical to CT, and all the residues interacting with lactose are identical in CT (Sixma et al., 1992). When CT is pre-incubated with lactose and tries to bind GM1, CT may be unable to dislodge the lactose. Lactose may block the saccharides from binding to their normal positions and displace them to a similar degree as when CT binds to GD1A.

When CT is pre-incubated with soluble GM1, the K_d is 764 ± 440 pM, 150 times larger than the K_d without the competitor. If soluble GM1 effectively competes with immobilized GM1, then one may imagine that a binding response should be eliminated. Several factors may contribute to the observed response. Since gangliosides form micelles in solution, the concentration of free GM1 would be less than 100 mM (Sonnino et al., 1994), thus some uninhibited CT might be present and therefore bind to immobilized GM1. A more likely explanation is that soluble GM1 incorporates into the sensor chip surface. It has been noted that if whole cells lacking a receptor for CT are incubated with soluble GM1, they acquire the ability to bind CT (Cuatrecasas, 1973a). When 100 μM samples of soluble GM1 were injected onto a sensor chip, we observed that some of the soluble GM1 incorporated into the lipid surface and produced a binding response.

The implication of this investigation is that CT specificity for gangliosides is not limited to the CT−GM1 interaction. We have shown that CT binds with very high affinity to multiple, structurally different gangliosides. It is possible that an inhibitor designed to inhibit the CT−GM1 interaction may inhibit just that interaction (CT−GM1), but still allow CT to bind to many other gangliosides that reside on the cell surface, perhaps causing damage in other ganglioside containing cells. Such a lack in understanding toxin−ganglioside interactions would greatly hinder vaccine development. This study also demonstrates the utility of using SPR with membrane-associated molecules. The cell surface can be reconstructed onto the hydrophobic sensor chips allowing receptor−ligand, receptor−lipid, and multivalency effects to be investigated.

ACKNOWLEDGMENT

We thank Russ Granzow, Shirley Demer, and Robert Schier for their technical assistance. We also thank the Marks lab, in particular Dr. Jim Marks, for the generous use of their BIAcore; likewise, we express our gratitude to the Schultz lab for allowing us gracious access to their facility. Finally, we thank Gary Wedemayer for help constructing figures and Cara Marks, Birgitte Andersen, Ken Goodwill, and Ned David for a critical reading of this manuscript.

REFERENCES

Cassel, D., & Pfeuffer, T. (1978) *Proc. Natl. Acad. Sci. U.S.A. 75*, 2669−2673.

Crothers, D. M., & Metzger, H. (1972) *Immunochemistry 9*, 341−357.

Cuatrecasas, P. (1973a) *Biochemistry 12* (18), 3547−3558.

Cuatrecasas, P. (1973b) *Biochemistry 12* (18), 3558−3566.

Degiorgio, V., Corti, M., & Giglio, M. (1980) *Light Scattering in Liquids and Macromolecular Solutions*, Plenum, New York.

Donta, S., & Viner, V. P. (1975) *Infect. Immun. 11*, 982−985.

Eidels, L., Proia, R. L., & Hart, D. A. (1983) *Microbio. Rev. 47*, 596−620.

Finklestein, R., Marchlewicz, B. A., MacDonald, R. J., & Boseman-Finklestein, M. (1983) *FEMS Microbiol. Lett. 17*, 239−241.

Fishman, P. H., Moss, J., & Osborne, J. C. (1978) *Biochemistry 17*, 711−716.

Fukuta, S., Magnani, J. L., Twiddy, E. M., Holmes, R. K., & Ginsberg, V. (1988) *Infect. Immun. 56*, 1748−1753.

Holmgren, J., Lonnroth, I., & Svennerholm, L. (1973) *Infect. Immun. 8*, 208−213.

Holmgren, J., Lonnroth, I., Mansson, J.-E., & Svennerholm, L. (1975) *Proc. Natl. Acad. Sci. U.S.A. 72* (7), 2520−2524.

Holmgren, J., Elwing, E., Fredman, P., & Svennerholm, L. (1980) *Eur. J. Biochem. 106*, 371−379.

Karlsson, R., Roos, H., Fagerstam, L., & Persson, B. (1994) in *Methods: A Companion to Methods in Enzymology*, Vol. 6, pp 99−110, Academic Press, San Diego, CA.

Kaufman, E. N., & Jain, R. K. (1992) *Cancer Res. 52*, 4157−4167.

Kooyman, R. P. H., Kolkman, H., Van Gent, J., & Greve, J. (1988) *Anal. Chim. Acta 213*, 35−45.

Lanne, B., Schierbeck, B., & Karlsson, K.-A. (1994) *J. Biochem. 116*, 1269−1274.

Malmqvist, M. (1994) *J. Mol. Recog. 6*, 1−7.

Masserini, M., Freire, E., Palestini, P., Calappi, E., & Tettamanti, G. (1992) *Biochemistry 31*, 2422−2426.

Merritt, E. A., Sarfaty, S., Van Den Akker, F., L'Hoir, C., Martial, J. A., & Hol, W. G. J. (1994) *Protein Sci. 3*, 166−175.

O'Shannessy, D. J., Brigham-Burke, M., Sonenson, K. K., Hensley, P., & Brooks, I. (1993) *Anal. Biochem. 212*, 457−468.

Pacuszka, T., Bradley, R. M., & Fishman, P. H. (1991) *Biochemistry 30* (10), 2563−2570.

Payne, G., Shoelson, S. E., Gish, G. D., Pawson, T., Walsh, C. T. (1993) *Proc. Natl. Acad. Sci. U.S.A. 90*, 4902−4906.

Plant, A. L., Brigham-Burke, M., Petrella, E. C., & O'Shannessy, D. J. (1995) *Anal. Biochem. 226*, 342−348.

Rosner, H., Al-Aqtum, M., & Rahmann, H. (1992) *Neurochem. Int. 20* (3), 339−351.

Schengrund, C.-L., & Ringler, N. J. (1989) *J. Biol. Chem. 264* (22), 13233−13237.

Schön, A., & Freire, E. (1989) *Biochemistry 28*, 5019−5024.

Sixma, T. K., Pronk, S. E., Kalk, K. H., van Zanten, B. A. M., Berghuis, A. M., & Hol, W. G. J. (1992) *Nature 355*, 561−564.

Sjölander, S., & Urbaniczky, C. (1991) *Anal. Chem. 63*, 2338−2345.

Sonnino, S., Cantu, L., Corti, M., Acquotti, D., & Venerando, B. (1994) *Chem. Phys. Lipids 71*, 21−45.

Spiegel, S. (1985) *Biochemistry 24*, 5947−5952.

Staerk, J., Ronneberger, H. J., Wiegandt, T., & Ziegler, W. (1974) *Eur. J. Biochem. 48*, 103−110.

Sternberg, E., Persson, B., Roos, H., & Urbaniczky, C. (1990) *J. Colloid Interface Sci. 143* (2), 513−526.

Walker, R., Caldwell, M. B., Lee, E. C., Guerry, P., Trust, T. J., & Ruiz-Palcios, G. M. (1981) *Microbiol. Rev. 50*, 81−94.

BI952314I